Large Impact Deformation Response of Spherical Shells

DONALD F. HASKELL*
Fairchild Hiller Corporation, Space and Electronics Systems Division, Germantown, Md.

A combination of experiment and simple theory is used to investigate the deformation response of complete, hollow spherical shells subjected at elevated temperature to high-velocity normal impact upon a planar rigid target. Temperature of the shells at impact is a few hundred degrees Fahrenheit below their melting point. A semi-inverse method of analysis is developed which is based upon energy conservation during the impact process. The method for prediction of dynamic behavior is essentially a static description of the deformation process. An assumed shell deformation pattern closely resembling the postimpact pattern obtained by test is used in formulating the external work and strain energy expressions. Consideration of one-dimensional stress wave propagation is used to develop the external work expression. Bending and stretching are included in the strain energy. A general expression for energy conservation is developed and subsequently considerably simplified by assuming the shell wall to behave as a rigid-linear strain hardening material. The average absolute difference between predictions of the analysis and test results is 8.6%.

Introduction

THIS investigation represents an initial attempt to develop an analytical method for predicting the deformation response of closed spherical shells subject to impact upon a planar rigid target. The need for such an analysis arises in the design of nuclear fuel containment capsules for spacecraft radioisotopic power generators. A principal nuclear safety constraint in spacecraft radioisotope fuel capsule design is the need for the fuel capsule to survive Earth impact at its terminal velocity in the event of launch abort or premature re-entry. This is necessary to prevent contamination of large areas of the earth's surface by nuclear fuel released from a ruptured fuel capsule. The conventional approach to this problem is to perform extensive design and test iterations until a design is achieved that satisfies the mission re-entry impact safety requirements. Such extensive developmental testing has been required in the past because adequate analytical tools for intact impact fuel capsule design have been unavailable.

Accurate prediction of the impact deformation of spherical shells is an exceedingly complex problem. This is particularly true for attempts to solve the governing equations for the deformation of a shell during impact in the conventional manner in which solutions to the "exact" equations are attempted for the actual three-dimensional (or even two-dimensional) continuous structure of the shell.

In recent years, broad impact test programs of cylindrical and spherical shells have been pursued. However, apparently because of the complexity of the problem, only a few analytical investigations have been undertaken and these have been relatively unsuccessful. In 1965, Young, Stoneking, and Colp[1] reported the results of one of these extensive shell impact test investigations. They performed an experimental study to determine the effect of length-to-diameter ratio and wall thickness on the rupture velocity of cylindrical, closed, partially filled radioisotope fuel containment capsules. The radius-to-thickness ratios of these cylinders ranged from 2.5 to 10.6, i.e., the shells ranged from thick to marginally thin shells. A total of 810 cylinders were subjected to axial impact against a one-cubic foot block of hardened SAE 4130 steel. A statistical analysis of the test results was performed from which a regression relation was obtained for rupture velocity in terms of cylinder length-to-diameter ratio and wall thickness. This relation did not include material property parameters and, therefore, could not relate rupture velocity with the characteristics of the shell material. The investigators concluded that, with other parameters held constant, rupture velocities increase as the thickness of the specimen tube wall increases and that rupture velocity decreases as the length-to-diameter ratio increases. In addition, they also concluded that there is no apparent relation between kinetic energy and rupture velocity.

Continued effort on shell impact response was reported by Stoneking, et al. in the following year. This effort concerned a theoretical analysis of cylindrical shells[2] as well as an experimental and theoretical investigation of spherical shells.[3] In Ref. 2, Oline and Stoneking reported a theoretical analysis of the response of hollow cylindrical shells to high-velocity axial impact and compared their predictions with the earlier test results of Ref. 1. Two separate analyses were performed. In one they employed elastic and plastic membrane analysis, and in the other, they used elastic bending theory. Failure velocity predictions based on the membrane theory were, on the average, 40% lower than the test failure velocities. Results of an attempt to compare the solutions of the proposed membrane and elastic bending analyses were stated to be inconclusive. This rather large difference between membrane theory predictions and the relatively thick shell impact test results is to be expected, especially since membrane theory is only strictly applicable to thin shells. In their conclusions, Oline and Stoneking acknowledge that one of the reasons for the differences between their theoretical failure velocities and the test failure velocities was caused by their use of the thin shell membrane theory.

In Ref. (3), Simonis and Stoneking reported the results of a theoretical and experimental study of the impact response of hollow spherical shells. As in his cylinder study, Stoneking proposed equations for failure velocity of hollow spheres based on membrane and bending theories. The failure velocities and associated maximum wall stresses in the spheres predicted by the proposed theory do not appear to be realistic however. Graphs were presented in the report illustrating the results of calculations for SAE 4130 steel spheres. The ultimate strength of this 4130 steel is reported to be approximately 100,000 psi. For a failure velocity of 125 fps the theory predicts 2,300,000 psi maximum capsule wall stress. Compared with the 100,000 psi ultimate strength of the steel,

Received January 8, 1970; revision received April 28, 1970. The theoretical portion of this work was sponsored by the Fairchild Hiller Corporation and the experimental portion was performed at Hittman Associates, Inc., for the U. S. Atomic Energy Commission under Contract AT(29-2)-2475.

* Senior Staff Engineer. Member AIAA.

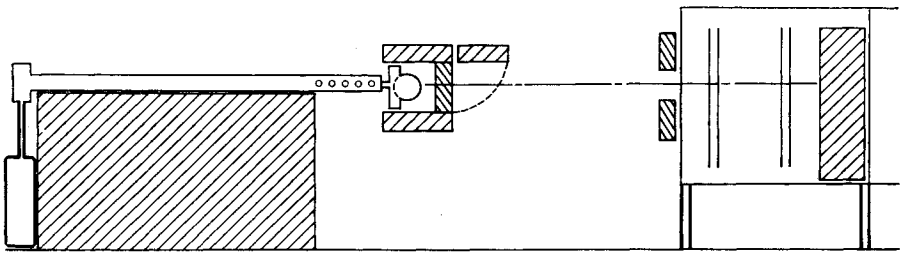

Fig. 1 Test arrangement.

this predicted maximum stress appears rather high. The theory also indicates a 25 fps failure velocity for a capsule with 0.1 in.-thick wall. For a 0.1 in.-thick wall this 25 fps failure velocity appears rather low and somewhat unrealistic. One of the major drawbacks of the analyses by Stoneking et al. in Refs. 2 and 3 is that their analyses are based on small deformation theory, whereas, in reality, capsules subject to re-entry impact undergo large, gross deformation. From this it appears physically impossible for small deformation theories to adequately describe the phenomena occurring during actual fuel containment capsule re-entry impact.

The present analytical approach utilizes a semi-inverse energy method of solution. In its development, the impact process is characterized by the law of conservation of energy. Approximate expressions for the work done by external forces during the impact and the shell strain energy are derived. An assumed deformation pattern which closely resembles the actual pattern observed through test is used to obtain the final form of the expressions. The external work expression is based upon the dynamic compressive stress developed by one-dimensional wave propagation. Bending and stretching deformations are employed to develop a general expression for the shell strain energy. Because of the gross deformation incurred by the impact process, elastic behavior of the material is neglected. The shell wall is assumed to be a rigid-linear strain hardening material. This allows the strain energy to be reduced to a simple expression which, when combined with the external work and kinetic energy in the conservation of energy relation, yields an explicit equation for the impact velocity required to produce a given deformation.

Predictions from this analysis and results of high-velocity impact tests conducted at elevated temperature are compared and found to be in good agreement. The average absolute difference between the analytical predictions and test results is 8.6%. The tests consisted of impacting closed thin shells upon a planar rigid surface at velocities ranging from 165 fps to 407 fps, while at a nominal temperature of 1800°F.

Test

Impact tests were performed on a total of sixteen Haynes-25 and Haynes-188 superalloy shells at a nominal temperature of 1800°F. Three of these shells were tested in the unaged condition with the remainder tested in an aged condition. Each complete shell was fabricated from two formed and machined hemispherical parts joined by a TIG (tungsten inert gas) weld. A gas gun was used to accelerate the shells for impact against a heavy, flat granite block.

Equipment and Impact Test Procedure

Basically, seven major components comprised the test equipment: a nitrogen gas gun with its gas supply chamber and control valves, a muzzle mounted furnace, sabot, sabot arrester, a 2 × 2 ft × 4 in. thick hard flat granite target block, a shell recovery box, and a velocity measurement system. A schematic of the test arrangement is shown in Fig. 1. The equipment shown in Fig. 1, the gun and its plenum chamber, furnace, sabot arrester, target block, and shell recovery box were housed in one room and a timer, furnace control, 6000 psi nitrogen storage bottle, and gas regulating valves in an adjacent control room. The walls of the gun room were constructed of concrete block and $\frac{1}{4}$-in.-thick steel plate.

The gun used to accelerate the shell consists of a smooth-bore barrel, breech assembly, solenoid controlled breech valve, pressure cylinder, control gage, and regulating valves, d-c voltage source, and steel-reinforced concrete base. All basic components are capable of operating up to 3000 psi. The barrel was made from a single piece of 4340 steel, heat treated and then bored and machined. The bore of the barrel is 6 ft long, with an inside diameter of 0.992 (+0.002, −0.000) in. and a straightness tolerance of 0.001 in. over the entire length. The muzzle end of the barrel has $\frac{1}{2}$-in. diameter ventholes, arranged in four rows of twelve each. These holes relieve the gas pressure immediately behind the sabot tube to end the accelerating portion of its flight while partially within the barrel. In this manner, a constant velocity is attained by the shell before it impacts the target block and the impact can be arranged to occur with part of the sabot tube still subject to guidance from the bore. This condition permits maximum accuracy in the alignment of the shell and target block.

The accelerating force is provided by compressed, dry nitrogen gas from a 6000 psi storage bottle sent at the desired pressure into the cylinder immediately behind the barrel and held in check by the breech valve. After the pressure has stabilized, the cylinder is sealed and the gun fired by applying a voltage pulse from the power supply to the breech valve. The valve opens, releasing the compressed gas into the barrel and pushing the sabot, like a piston, down the barrel.

The sabot is a 3 ft by 0.991 (−0.001) in. diam by $\frac{1}{16}$-in. thick wall aluminum tube closed at one end with a 3 in. or 5 in. diam (depending on the diameter of the shell to be tested) by $\frac{1}{16}$-in. thick circular aluminum plate welded to the other end. Attached to the flat front end of this circular plate is a 1 in. thick by 3 in. (or 5 in.-)diam low-density, silica foam thermal insulation disk. The shell to be tested is mounted in a cavity in the front of the disk of radius equal to the radius of the shell to be tested. This silica foam disk serves both as thermal insulation and holder for the shell. As an insulator it forms the rear door of the muzzle mounted shell furnace and also acts as a barrier to heat transfer into the aluminum sabot tube.

The shell furnace is an open-ended cylindrical electrical resistance furnace mounted on the muzzle end of the gun barrel and aligned with the gun axis. The aft (or muzzle) end of the furnace is closed by the silica foam insulation disk on the sabot when the sabot is fully loaded into the gun. The front end of the furnace is closed by a quick retraction door. The shell to be impact tested is mounted in the sabot which is loaded into the muzzle end of the gas gun. The retractable front door of the furnace is then closed and the shell is heated to its test temperature. The test is initiated by opening the quick retraction front door of the furnace and activating the quick release gas gun valve. The sabot and shell are fired directly through the horizontal furnace chamber. The shell is separated from its sabot by the sabot arrester which stops the sabot, allowing the shell to fly free through a circular opening

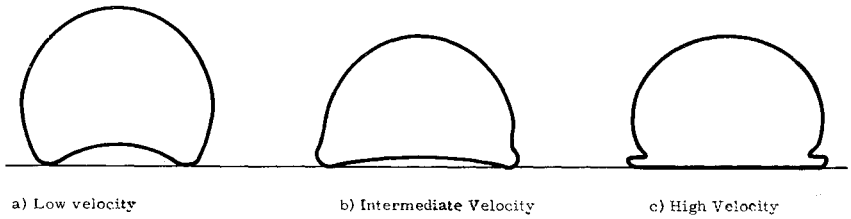

Fig. 2 Typical deformation patterns: a) low velocity; b) intermediate velocity; c) high velocity.

in the arrester. After passing through two timing "gates" the shell impacts against the flat granite target within the recovery box. Soft, cotton-like thermal insulation lining the recovery box keeps the impacted shell from suffering post-impact damage from secondary impacts. Flight distance of the shell is approximately 6 ft from its position in the furnace at the muzzle end of the gun to the face of the target block.

Velocity of the shell is measured just before impact by the timing "gates." It is determined by measuring the time in microseconds for the shell to pass between two reference points located a set distance apart. A timer is started by a voltage pulse produced when the shell passes the first reference point, or gate, and stopped by another voltage pulse when the shell passes the second reference point. This is accomplished by two wire gates in a timer circuit. Each gate consists of two sets of fine parallel copper wires with the wires of one set perpendicular to the wires of the other set. The parallel wires within one set are approximately $\frac{1}{32}$ in. apart with the two perpendicular sets of each gate separated by $\frac{1}{2}$ in. The two sets of wires in each gate perform as a timer activation switch. As the oncoming shell brushes the wires of the upstream set of wires in one gate into contact with the adjacent downstream perpendicular set, the timer count is initiated. The count is stopped and the time of flight between the two gates obtained, as the shell passes through the downstream gate. With the 13.5 in. between gates measured to at least $\frac{1}{32}$ in. accuracy and the timer accurate to ± 1 μsec, the nominal accuracy in velocity for a 500 fps maximum test velocity is approximately $\pm 0.27640\%$ or ± 1.38 fps.

The test procedure was as follows. The shell was mounted in its sabot and the sabot muzzle-loaded into the gun. The shell was then heated to its desired temperature by the muzzle mounted furnace. Shell temperature was determined by a thermocouple in contact with the shell. Five minutes after the shell attained temperature equilibrium, the furnace port was opened and the sabot and shell fired directly through the furnace. The shell was separated from its sabot by the sabot arrester, passed through the wire screen timing gates, and then impacted the flat granite target block inside the recovery box. After impact, the shells were sectioned through the axis of impact. A tracing of the post impact deformation pattern of the shell was then obtained. Table 1 lists the radial shell displacement of shell 1 as measured around the periphery of the shell. Typical deformation patterns are illustrated by Fig. 2. Test results along with analytical predictions are listed in Table 2.

Mechanical Properties of Shell Materials

Tensile tests of the shell materials were performed on both unaged and aged specimens. In order to obtain good correlation between theory and test, an attempt was made to obtain both impact test shell material and tensile test coupons from the same heat. However, it was not possible to obtain both tensile test specimens and shell material from the same heat for the Haynes-25 alloy. For Haynes-25, the tensile specimens and shells were obtained from two separate but chemically similar alloy heats. Yield strength, ultimate tensile strength, elongation over a 1-in. gage length, and modulus of elasticity were the properties measured. The aged material was aged in air at 1500°F—the Haynes-188 alloy for 500, and the Haynes-25 for 482 hr. Both aged and unaged specimens were tensile tested over a temperature range from 70°F to 2200°F. The actual test temperatures were 70°, 1300°, 1800°, 2000°, 2100°, and 2200°F. From a plot of these test results, the alloy properties at the particular impact test temperature were obtained as listed in Table 2. The tests were conducted in a Tinius-Olsen universal testing machine. A load-elongation curve was recorded for each test on a Tinius-Olsen autographic recorder incorporated into the testing machine. At the nominal test temperature of 1800°F, an Inconel extensometer frame was used to transmit the axial strains of the specimen gage section outside the furnace to a Tinius-Olsen S-1 extensometer.

The furnace was a three-zone, resistance wound, split tube furnace mounted on the testing machine. Specimen temperatures were measured with 36 gage (0.005-in. diam) chromel-alumel thermocouples "spot" welded to the top and bottom of the specimen gage section and read with a Leeds and Northrup direct-reading potentiometer.

The tests were conducted in accordance with ASTM Specifications E 8-66 and E 21-66T. The general testing procedure at 1800°F was as follows. Each specimen was heated in air to 1800°F ± 5°F and held at temperature for about 5 min. After the hold time, the specimen was loaded in tension at a strain rate of approximately 0.005 in./in./min to 0.6% strain and at 0.05 in./in./min from 0.6% strain to fracture.

Discussion of Test Results

The shells were impacted at velocities in the range from $\frac{1}{36}$ to $\frac{1}{14}$ of the material elastic wave velocity. At 1800°F the elastic wave velocity of unaged Haynes-25 alloy is approximately 5,980 fps. A total of fifteen shells were tested over this velocity range. Three of these shells buckled at impact while the remaining twelve simply deformed without formation of circumferential buckles in the shell wall. Two of these three buckled shells were very thin shells with a radius-to-thickness ratio of 66.6. Radius-to-thickness ratios of the other shells ranged from 20 to 40. The third shell that buckled at impact (with a radius-to-thickness ratio of 40) was impacted at the highest velocity of its particular radius-to-thickness ratio group.

Table 1 Meridional radial displacement of shell 1[a]

Colatitude ϕ	0°	10°	20°	30°	40°	50°	60°	70°	80°	90°
+	...	−0.6750	−0.6560	−0.6200	−0.5525	−0.4430	−0.2190	+0.0979	0	0
−	...	−0.6670	−0.6560	−0.6200	−0.5575	−0.4530	−0.2500	+0.0833	+0.0417	0
Av.	−0.6820	−0.6710	−0.6560	−0.6200	−0.5550	−0.4480	−0.2355	+0.0906	+0.0208	0

[a] The displacements (in inches) are measured from the initial profile of the spherical midsurface before impact.

Table 2 Shell impact test results[a]

Shell number	R/t	Impact temp., °F	σ_y, ksi	σ_u, ksi	e_f, in./in.	E, 10^6 psi	$\bar{E}$, 10^3 psi	f, d/r	Impact velocity, fps: Test	Impact velocity, fps: Theory	Difference %
Haynes-25											
1*	28.5	1892	22.0	22.2	0.35	6.0	10.3	0.594	337	343	+1.8
2	28.5	1772	25.0	28.6	0.32	4.5	11.25	0.313	165	194	+17.6
3	28.5	1827	23.0	26.4	0.31	4.3	10.3	0.598	390	358	−8.2
4	28.5	1827	23.0	26.4	0.31	4.3	10.3	0.719	405	485	+19.7
Haynes-188											
5*	20.0	1800	21.9	25.4	0.56	9.0	6.2	0.563	368	371	+0.8
6	33.3	1800	23.3	27.2	0.55	7.6	7.1	0.500	308	299	−2.9
7	20.0	1800	23.3	27.2	0.55	7.6	7.1	0.531	400	356	−11.0
8	20.0	1800	23.3	27.2	0.55	7.6	7.1	0.531	402	356	−11.4
9	20.0	1800	23.3	27.2	0.55	7.6	7.1	0.625	407	431	+5.9
10*	40.0	1820	21.4	23.8	0.56	8.9	4.29	0.427	295	278	−5.9
11	40.0	1820	22.0	24.5	0.54	7.4	4.63	0.493	307	286	−6.8
12	40.0	1800	23.3	27.2	0.55	7.5	7.1	0.406	264	234	−11.4
13	66.6	1813	22.3	25.0	0.54	7.4	5.0	0.500	286	Buckled around	
14	66.6	1810	22.3	25.0	0.54	7.4	5.0	0.593	305	periphery of	
15	40.0	1804	23.3	27.2	0.55	7.5	7.1	0.469	278	shell	

[a] The aging treatments consisted of aging in air at 1500° F: 482 hr for Haynes-25 and 500 hr for Haynes-188. The shells marked * were tested in the unaged condition. Average absolute error between test and theory = 8.6%.

The deformed shape of the shells was found to fall into one of three general patterns as illustrated by Fig. 2. These patterns appear related to shell radius, thickness, modulus of elasticity, impact velocity, and material strength. The first pattern, Fig. 2a, is concave inward at the impacted region and occurs with thick shells or low impact velocity. The second and third patterns are characteristic of thin shells and/or high impact velocity. Of these, the pattern shown by Fig. 2b is produced at intermediate velocity with the third pattern (Fig. 2c) occurring at high impact velocity. The second pattern is characterized by a relatively flat impacted region. Bulges appear around the periphery of this flat region as velocity is increased until a critical velocity is reached at which buckles form around the periphery of the flattened region in the direction of impact. At even higher velocity cracks begin to appear within the "folds" of these buckles.

On all shells tested, the aft region appeared to be little affected by the impact. Within the accuracy of the measurements, the permanent deformation in this aft region is essentially zero. Consequently, it may be safely concluded that the major portion of the work performed in stopping the shell is absorbed within the shell-target contact region.

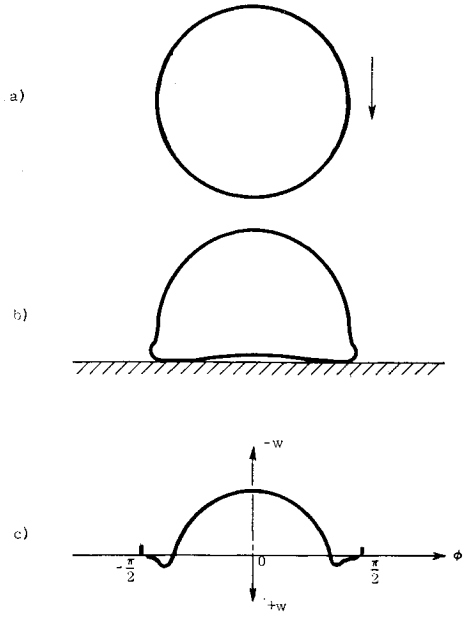

Fig. 3 Radial displacement pattern of shell 1.

Theory

As described by Sokolnikoff,[4] "the work W done by the external forces in altering the configuration of the natural (or unstrained) state to the state at time t is equal to the sum of the kinetic energy K and the strain energy U. The strain energy U may be conceived as the energy stored in the body when it is brought from the configuration of the natural state to the state at the time t." This simple description of the law of conservation of energy may be expressed by the equation

$$W = K + U \tag{1}$$

The function W, K, and U, are defined as follows:

$$W = \iint [u\bar{X} + v\bar{Y} + w\bar{Z}] \cdot dA \text{ (Ref. 5)} \tag{2}$$

$$K = \tfrac{1}{2}m(v_f^2 - v_i^2) \tag{3}$$

$$U = \int_V \bar{U} \cdot dV \tag{4}$$

where u, v, w = displacement in the meridional, circumferential, and radial directions, respectively; $\bar{X}, \bar{Y}, \bar{Z}$ = external stresses in the u, v, and w direction, respectively; A = surface area of the body over which the external forces are applied; m = mass of the body; v_f, v_i = final and initial velocities of the body; $\bar{U}$ = strain energy volume density, or elastic potential; U = strain energy; and V = volume of the body.

The time interval over which this relation is applied is from an instant immediately preceding impact to the time after impact when the shell has come to rest. Since the final veloc-

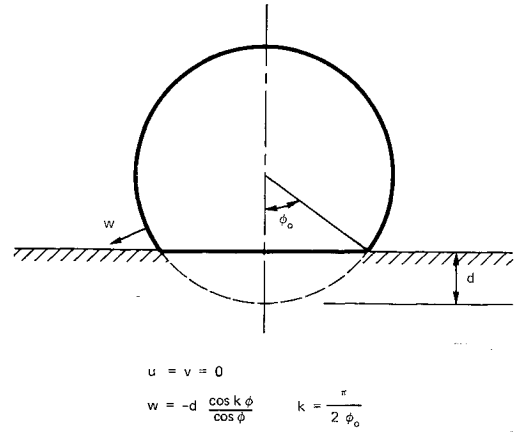

Fig. 4 Assumed displacement pattern.

ity of the shell is zero, the kinetic energy function is

$$K = -\tfrac{1}{2}mv_i^2 \tag{5}$$

where v_i is the shell velocity at impact. For a hollow shell of thickness t, radius R and shell wall material density ρ, the kinetic energy function is

$$K = -2\pi R^2 t\rho v_i^2 \tag{6}$$

The work done by the external forces during impact and the strain energy stored in the shell may be evaluated by considering the shell's postimpact deformation pattern. Normal impact upon a planar rigid surface results in axisymmetric deformation. In this case $u = v = 0$. Since the impacted region of the shell is essentially a plane surface normal to the direction of impact (see Figs. 3 and 4), deformation normal to the shell may be approximated by the function

$$w = -d(\cos k\phi/\cos\phi) \tag{7}$$

where d = displacement amplitude, $k = \pi/2\phi_0$, $\phi_0 = \cos^{-1}(1 - f)$, $f = d/R$.

During the impact event, the external stress acting on the shell p is equal to the stress pulse in the deforming shell. In terms of the impact velocity and the plastic wave velocity of the shell material, this dynamic compressive stress pulse is $p_d = -\tfrac{1}{2}\rho C_p v_i$, where ρ = mass density of shell material and C_p = plastic wave velocity. Since $C_p = (\bar{E}/e)^{1/2}$ the stress pulse is

$$p_d = \tfrac{1}{2}(\bar{E}\rho)^{1/2}v_i \tag{8}$$

As the shell decelerates this stress decreases. Because the exact decay form of this stress pulse is not available, the stress pulse is assumed to be a linearly decreasing function of ϕ, the angle between the normal to the shell middle surface and the axis of impact (see Fig. 5)

$$p = p_d(1 - \phi/\phi_0) \tag{9}$$

As the shell flattens against the target surface this stress is applied to the oncoming portion of the shell over an annular incremental area around the periphery of the circular flattened portion of the shell. This incremental area is

$$dA = 2\pi R^2 \sin\phi\cdot d\phi \tag{10}$$

The component of the applied stress in the radial displacement direction is given by

$$\bar{Z} = p\cos\phi \tag{11}$$

which, after substitution of Eqs. (8) and (9), becomes

$$\bar{Z} = -\tfrac{1}{2}(\bar{E}\rho)^{1/2}v_i(1 - \phi/\phi_0)\cos\phi \tag{12}$$

By substituting Eqs. (7, 12, and 10) into Eq. (2) with $u = v = 0$ the general expression for work done by the external force during the impact event becomes

$$W = \pi R^2 d(\bar{E}\rho)^{1/2}v_i \int_0^{\pi}\left(1 - \frac{\phi}{\phi_0}\right)\sin\phi\cdot\cos k\phi\cdot d\phi \tag{13}$$

As indicated by Fig. 3, most of the shell deformation is incurred in the flattened front portion of the shell. Very little plastic deformation occurs in the aft portion that does not contact the flat target surface. Comparison of shell profiles before and after impact indicates practically zero plastic deformation in this aft portion. Consequently, as a first approximation, the integration indicated by Eq. (13) need only be performed from $\phi = 0$ to $\phi = \phi_0$, i.e., over the visibly flattened portion. In this case, the work done by the external forces is given by

$$W = \pi R^2 d(\bar{E}\rho)^{1/2}v_i \int_0^{\phi_0}\left(1 - \frac{\phi}{\phi_0}\right)\sin\phi\cdot\cos k\phi\cdot d\phi \tag{14}$$

After expanding the trigonometric terms in series form, multiplying these series, and neglecting all terms in the resulting series expansion except the first two terms, the integral is readily evaluated with the resultant expression for W obtained as follows:

$$W = \frac{\pi}{2}R^2 d(\bar{E}\rho)^{1/2}\phi_0^2\left[\frac{1}{3} - \frac{(1 + 3k^2)}{20}\phi_0^2\right]v_i \tag{15}$$

The term in the conservation of energy statement that remains to be evaluated is the shell strain energy U. For a thin spherical shell

$$U = R^2\int_0^{\pi}\int_{-t/2}^{t/2}\int_0^{2\pi}(\sigma_\phi e_\phi + \sigma_\theta e_\theta + \tau_{\phi\theta}e_{\phi\theta} + \tau_{\phi z}e_{\phi z} + \tau_{\theta z}e_{\theta z})\cdot\sin\phi\cdot d\theta\cdot dz\cdot d\phi \tag{16}$$

where $\sigma_\phi, \sigma_\theta$ = normal stresses in the ϕ and θ directions, respectively; $\tau_{\phi\theta}$ = shear stress in the shell midsurface; $\tau_{\phi z}, \tau_{\theta z}$ = transverse shear stresses; e_ϕ, e_θ = normal strains in the ϕ and θ directions, respectively; $e_{\phi\theta}$ = midsurface shear strain; $e_{\phi z}, e_{\theta z}$ = shear strains transverse to the shell midsurface. Expressions for the strains that include bending and midsurface stretching for finite axisymmetric deformations are[6]

$$e_\phi = \omega/R + \omega'^2/2R^2 + (z/R^2)\omega'' \tag{17a}$$

$$e_\theta = \omega/R + (z/R^2)\omega'\cot\phi \tag{17b}$$

$$\gamma_{\phi\theta} = 0 \tag{17c}$$

$$\gamma_{\phi z} = \omega'/R \tag{17d}$$

$$\gamma_{\theta z} = 0 \tag{17e}$$

where $(\ )' = d(\ )/d\phi$ and $(\ )'' = d^2(\ )/d\phi^2$. The shell wall is assumed to be a rigid-linear strain hardening material as illustrated by Fig. 6. The material is assumed to behave in this manner because the shell undergoes gross plastic deformation during impact. Elastic contribution to this overall deformation is extremely small; it may be shown for a given deformation that the elastic portion of the material

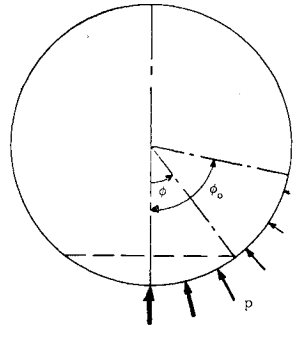

Fig. 5 Linearly varying stress pulse.

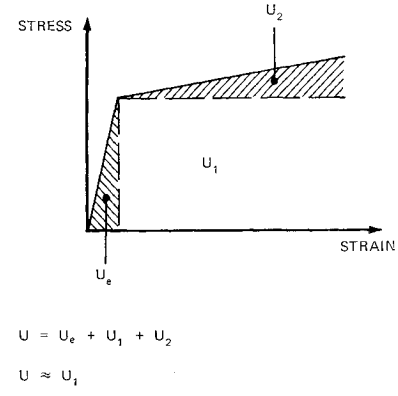

Fig. 6 Internal strain energy partition for rigid-linear strain hardening material.

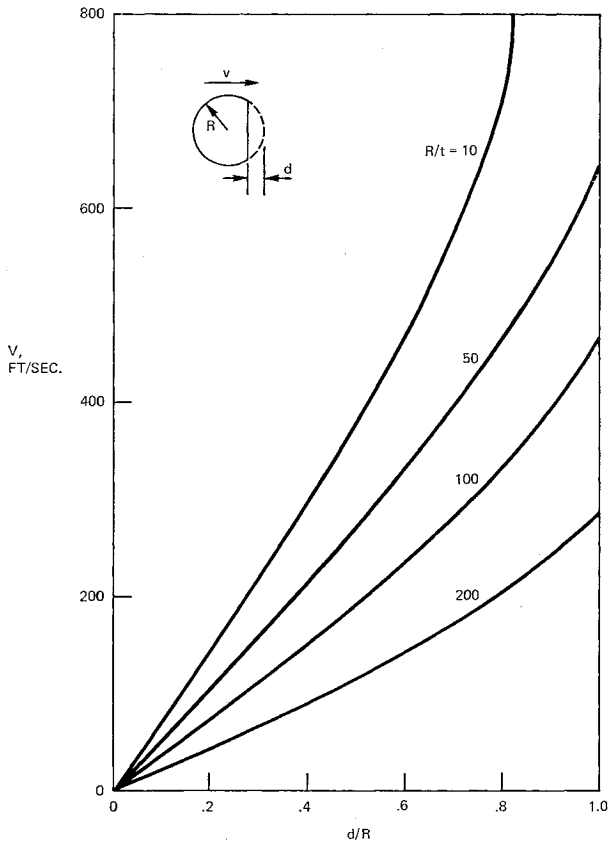

Fig. 7 Impact velocity vs deformation for various radius-to-thickness ratios; $\sigma_y/\rho = 30 \times 10^6$ in.^{2}/sec^2, $\bar{E}/\rho = 10^6$ in.^{2}/sec^2.

behavior contributes only 1.8% to the shell impact velocity. Therefore, it is considered reasonable to neglect the contribution of elastic deformation in the formulation of a first-order theory. The main concern here is to account for the over-all gross deformation. Consequently, the stress-strain behavior is expressed by the relations

$$\sigma_\phi = \sigma_y + \bar{E}e_\phi \tag{18a}$$

$$\sigma_\theta = \sigma_y + \bar{E}e_\theta \tag{18b}$$

$$\tau_{\phi\theta} = \tau_y + \bar{G}\gamma_{\phi\theta} \tag{18c}$$

$$\tau_{\phi z} = \tau_y + \bar{G}\gamma_{\phi z} \tag{18d}$$

in which σ_y,τ_y = normal and shear yield stress, respectively; $\bar{E} = (\sigma_u - \sigma_y)/e_f$; $\bar{G} = (\tau_u - \tau_y)/\gamma_f$; σ_u,τ_u = ultimate normal and shear strengths, respectively; and e_f,γ_f = maximum normal and shear strains, respectively.

If the stress-strain relations expressed by Eqs. (18) are substituted into Eq. (16) and integration with respect to θ is performed, the shell strain energy expression becomes

$$U = 2\pi R^2 \int_0^\pi \int_{-t/2}^{t/2} [\sigma_y(e_\phi + e_\theta) + \tau_y(\gamma_{\phi\theta} + \gamma_{\phi z})] \times \sin\phi \cdot dz \cdot d\phi + 2\pi R^2 \int_0^\pi \int_{-t/2}^{t/2} [\bar{E}(e_\phi{}^2 + e_\theta{}^2) + \bar{G}(\gamma_{\phi\theta}{}^2 + \gamma_{\phi z}{}^2)] \sin\phi \cdot dz \cdot d\phi \tag{19}$$

Let

$$U_1 = 2\pi R^2 \int_0^\pi \int_{-t/2}^{t/2} [\sigma_y(e_\phi + e_\theta) + \tau_y(\gamma_{\phi\theta} + \gamma_{\phi z})] \sin\phi \cdot dz \cdot d\phi$$

$$U_2 = 2\pi R^2 \int_0^\pi \int_{-t/2}^{t/2} [\bar{E}(e_\phi{}^2 + e_\theta{}^2) + \bar{G}(\gamma_{\phi\theta}{}^2 + \gamma_{\phi z}{}^2)] \times \sin\phi \cdot dz \cdot d\phi$$

then

$$U = U_1 + U_2 \tag{20}$$

Substitution of the strain-displacement relations, Eq. (17), into these energy expressions and integration with respect to z results in the following relations for U_1 and U_2:

$$U_1 = 2\pi R^2 t \int_0^\pi \left[\sigma_y\left(\frac{2w}{R} + \frac{w'^2}{2R^2}\right) + \tau_y\left(\frac{w'}{R}\right)\right] \times \sin\phi \cdot d\phi \tag{21a}$$

$$U_2 = 2\pi R^2 t\bar{E} \int_0^\pi \left(\frac{2w^2}{R^2} + \frac{ww'^2}{R^3} + \frac{w'^4}{4R^4}\right) \sin\phi \cdot d\phi + \frac{\pi R^2 t^3}{6} \bar{E} \int_0^\pi \left(\frac{w''^2}{R^4} + \frac{w'^2 \cot^2\phi}{R^4}\right) \sin\phi \cdot d\phi + 2\pi R^2 t\bar{G} \int_0^\pi \frac{w'^2}{R^2} \sin\phi \cdot d\phi \tag{21b}$$

If the analysis is restricted to impacts with resultant amplitudes less than the shell radius, all terms involving the deflection w or its derivatives of order greater than one will be small relative to the first-order terms. Consequently, if the terms of order two and above are neglected, the strain energy reduces to the following form involving only U_1;

$$U = 2\pi R^2 t \int_0^\pi \left[\sigma_y\left(\frac{2w}{R}\right) + \tau_y\left(\frac{w'}{R}\right)\right] \sin\phi \cdot d\phi \tag{22}$$

As before, the integration need only be taken from zero to ϕ_0 since the remainder of the shell receives little or no plastic deformation. After changing the upper integration limit to ϕ_0 and substituting the deflection and its derivative from Eq. (7) into Eq. (22), the strain energy stored in the shell during the impact event is given by

$$U = 2\pi R^2 tf \int_0^{\phi_0} [-2\sigma_y \cos k\phi \tan\phi + \tau_y (k \sin k\phi \tan\phi - \cos k\phi \tan^2\phi)] \cdot d\phi \tag{23}$$

If the trigonometric terms are expanded in series form, multiplied as required, and then integrated after neglecting terms of order four and higher, the approximate strain energy reduces to the following:

$$U = 2\pi R^2 tf[2\sigma_y \ln(1 - f) - \tfrac{1}{3}\tau_y\phi_0{}^3] \tag{24}$$

It is to be noted that, by definition, strain energy is a positive quantity.

Now that expressions for the kinetic energy, external work, and strain energy functions have been obtained, a statement of the conservation of energy throughout the impact event may be formulated. Equations (1, 6, 15, and 24) are rewritten here for conciseness,

$$K - W + U = 0 \tag{1a}$$

$$K = -(2\pi R^2 t\rho)v_i{}^2 \tag{6a}$$

$$W = \frac{\pi}{2} R^2 d\,(\bar{E}\rho)^{1/2}\,\phi_0{}^2[\tfrac{1}{3} - \tfrac{1}{20}(1 + 3k^2)\phi_0{}^2]v_i \tag{15a}$$

$$U = 2\pi R^2 tf[2\sigma_y \ln(1 - f) - \tfrac{1}{3}\tau_y\phi_0{}^3] \tag{24a}$$

Substituting Eqs. (6, 15, and 24) into (1a), the statement of energy conservation, and dividing by the coefficient of the $v_i{}^2$ term yields the following quadratic equation:

$$v_i{}^2 + \left[\frac{1}{12}\frac{R}{t} f\phi_0{}^2 \left(\frac{\bar{E}}{\rho}\right)^{1/2} \left(1 - \frac{1 + 3k^2}{20}\phi_0{}^2\right)\right] v_i - \frac{f}{\rho}\left[2\sigma_y \ln(1 - f) - \frac{1}{3}\tau_y\phi_0{}^3\right] = 0 \tag{25}$$

From this relation, the impact velocity v_i that causes a specified amount of deformation f may be determined. Letting

$$B = \frac{1}{12}\frac{R}{t} f\phi_0^2 \left(\frac{\bar{E}}{\rho}\right)^{1/2} \left(1 - \frac{1 + 3k^2}{20}\phi_0^2\right) \quad (26)$$

$$C = 4(f/\rho)[2\sigma_y \ln(1 - f) - \tfrac{1}{3}\tau\phi_0^3] \quad (27)$$

and for simplicity,

$$\tau_y = \sigma_y/(3)^{1/2} \quad (28)$$

so that

$$C = 4f(\sigma_y/\rho)[2 \ln(1 - f) - (3^{1/2}/9)\phi_0^3] \quad (29)$$

the solution of Eq. (25) may be written in the following manner:

$$v_i = \tfrac{1}{2}[-B + (B^2 + C)^{1/2}] \quad (30)$$

As a consequence of the particular sign convention employed for the deflection in this treatment, the apparent calculated value of C is negative. However, this is only apparent since strain energy is a positive quantity and as such C must also be a positive quantity.

Discussion of Analytical Results

Figures 7 and 8 illustrate some of the results of the analysis. In these figures, the curves representing the shell impact velocity required to incur a certain amount of radial deformation have been calculated from Eq. (30). These curves are for typical superalloy shells impacted at 1800°F. Figure 7 shows impact velocity variation with deformation for shells of various thicknesses. As expected, deformation increases as velocity increases and shell thickness decreases. Deformation increases rapidly as velocity is increased from low values. However, at high velocities, the velocity-deformation envelope curves toward the velocity axis, showing that the rate of deformation decreases with increasing velocity. Figure 8 illustrates the effect of deformation. Again, thin shells are shown to deform more at a given velocity than thick shells. The velocity required to produce a given deformation decreases markedly as thickness decreases.

Comparison of Analytical and Test Results

Table 2 lists predictions obtained by Eq. (30), along with the test results. This table lists the shell impact velocity and its deformation f (indicated by the ratio of maximum radial deformation to shell radius). The table also lists the theoretical impact velocity required to produce the same deformation incurred by test. The difference between the test and theoretical velocities ranges from −11.4% (theory lower than test) to +19.7% (theory higher than test). The over-all absolute difference between theory and test is 8.6%. This shows good agreement between theory and test and serves to indicate the success of the semi-inverse energy method of analysis.

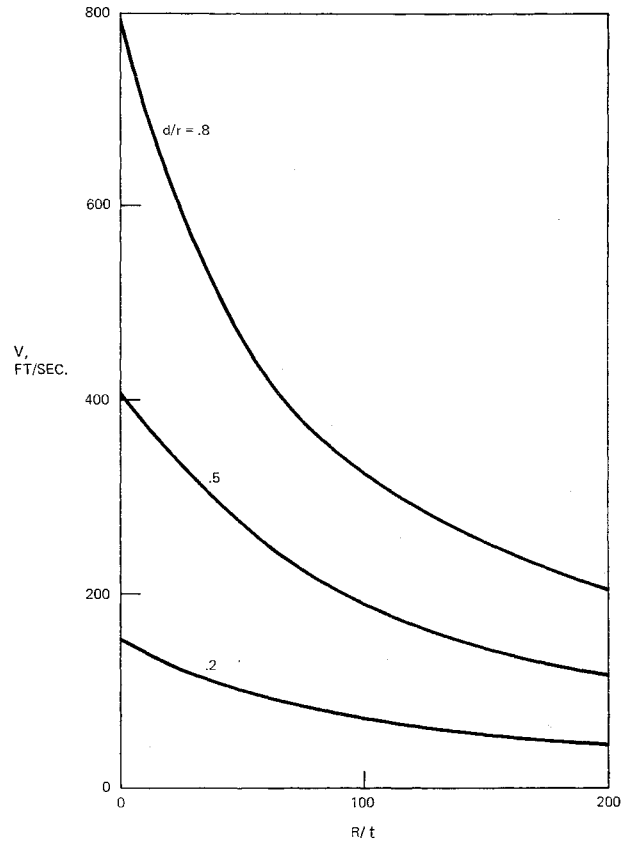

Fig. 8 Impact velocity vs shell thickness for various amounts of deformation; $\sigma_y/\rho = 30 \times 10^6$ in.^{2}/sec^2, $\bar{E}/\rho = 10 \times 10^6$ in./^{2}sec^2.

References

[1] Young, C. W., Stoneking, C. E., and Colp, J. L., "Containment Capsule Impact Safety Study, Phase A, Progress Report," SC-RR-65-9, July 1965, Sandia Corp., Albuquerque, New Mexico.

[2] Oline, L. W. and Stoneking, C. E., "A Study of Impact Effects on Spherical Shells—Part I. A Theoretical Study of the Response of Hollow Cylinders to Impact Loads," SC-CR-66-2135, Nov. 1966, Sandia Labs., Albuquerque, New Mexico.

[3] Simonis, J. C. and Stoneking, C. E., "A Study of Impact Effects of Spherical Shells—Part II. A Theoretical and Experimental Study of the Response of Spherical Shells to Impact Loads," SC-CR-67-2540, Dec. 1966, Sandia Labs., Albuquerque, New Mexico.

[4] Sokolnikoff, I. S., *Mathematical Theory of Elasticity*, 2nd edition, McGraw-Hill, New York, 1956, p. 83.

[5] Wang, C-T., "Principle and Application of Complementary Energy Method for Thin Homogeneous and Sandwich Plates and Shells with Finite Deflections," TN 2620, Aug. 1949, NACA.

[6] Baker, E. H. et al., *Shell Analysis Manual*, NASA CR-912, April 1968, North American Aviation, Inc., Downey, Calif.